RESEARCH ARTICLE

Polycaprolactone scaffold as targeted drug delivery system and cell attachment scaffold for postsurgical care of limb salvage

Bin Sheng Wong · Swee-Hin Teoh · Lifeng Kang

Abstract In this paper, a dual-function drug-laden polycaprolactone scaffold, which can serve as both targeted drug delivery system and attachment platform for tissue regeneration for the postsurgical care of limb salvage procedure, was developed with a simple and solvent-free molding technique. Scaffolds of varying surface architecture were created using poly(ethylene glycol) diacrylate microneedle arrays. A model drug, rhodamine B, was incorporated homogenously into the scaffold. In vitro drug release studies showed that rhodamine B was released in a slow and sustained manner for 112 days. Its release rate was affected by drug loading and scaffold surface architecture. Release of rhodamine B from the scaffolds followed the Higuchi diffusion model. Other drugs, namely, doxorubicin and lidocaine hydrochloride, were also effectively loaded into and released from the scaffolds. Cell attachment study demonstrated potential for the scaffolds to provide attachment platforms for tissue regeneration.

Keywords Scaffold · Polycaprolactone · Targeted drug delivery · Tissue engineering

B. S. Wong · L. Kang (✉)
Department of Pharmacy, National University of Singapore,
18 Science Drive 4,
Singapore 117543, Singapore
e-mail: lkang@nus.edu.sg

S.-H. Teoh
Division of Bioengineering, School of Chemical and Biomedical Engineering, Nanyang Technological University,
70, Nanyang Drive,
Singapore 637457, Singapore

Introduction

Limb salvage procedure is a type of surgery that involves local resection of bone or soft tissue cancers in order to avoid amputation [1]. This procedure has proven to be effective in the treatment of osteosarcoma due to its superior ability to maintain the external appearances and physiological functions of the patients' limbs [2, 3]. Typically, the surgery involves the removal of tumors and some surrounding tissues, followed by the placement of either metal prosthesis or bone graft in the resected space to provide mechanical support and platform for bone regeneration. The use of metal prosthesis, however, is plagued with numerous limitations such as corrosion [4], metal hypersensitivity [5], stress shielding [6], growth restriction [7], imaging interference [8], and the need for additional removal operation [9]. The usage of bone grafts is also not ideal because allograft is often associated with nonunion, infection, disease transmission, and limited donor availability [10, 11]. While autograft can circumvent the problem of disease transmission and tissue incompatibility, it is limited by donor site morbidity, increased operative time, and chronic pain [11, 12]. Biodegradable implants, therefore, emerged as viable alternatives for limb salvage procedure and have since demonstrated promising results in bone regeneration of cranioplasty and bone defects [13, 14].

Often, chemotherapy is given to patients following a limb salvage procedure to destroy any lingering microscopic deposits of the malignant cells and reduce cancer recurrence [15]. While chemotherapy has proven to be highly effective in increasing the disease-free survival rate of localized osteosarcoma [16], conventional systemic chemotherapy is unfortunately highly toxic [17]. Aside from postoperative chemotherapy, radiotherapy is also used in patients following surgical resection to minimize cancer recurrence. While radiotherapy is considered generally safe and effective, it

also possesses several disadvantages such as soft tissue damage, increased pain, and the need for additional orthopedic procedures. Some bone cancer cells also do not respond well to radiotherapy [18]. One major complication following a limb salvage procedure is surgical wound and orthopedic device infections [19]. Hence, oral or intravenous broad-spectrum antibiotics are regularly prescribed to prevent or treat infections associated with limb salvage surgeries. Patients often receive prophylactic anticoagulants to prevent the formation of thrombus and embolus postsurgery. Opioids, mild narcotics, anti-inflammatory, and other analgesics are also sometimes given to patients to counter pain experienced following the surgery [20].

To minimize systemic drug toxicities, especially for the cytotoxic agents and antibiotics, and to ensure adequate supply of the various therapeutic agents, a targeted and controlled drug delivery system can be designed. By encapsulating drugs in micropolymeric or nanopolymeric structures, targeted drug delivery allows drugs to remain at specific sites of action at sufficiently high concentration to exert their pharmacological effects, without causing severe systemic toxicities. Additionally, targeted drug delivery also improves drug absorption and intracellular penetration, prolongs retention time, enhances drug efficacy, and reduces drug degradation [21].

In view of the existing challenges and limitations of limb salvage surgery, a novel biodegradable and drug-laden polymeric scaffold was envisioned to serve as viable alternative to metal prostheses and bone grafts to promote bone and tissue regeneration and to simultaneously function as a targeted and controlled drug delivery system for the drugs that patients would typically receive after a limb salvage surgery to minimize undesirable systemic toxicities.

Polycaprolactone (PCL), due to its nontoxic, inert, biodegradable, and biocompatible nature [22], has been gaining significant popularity in the field of targeted drug delivery. Numerous drugs, such as cisplatin, doxorubicin, and gentamicin sulfate, have been successfully incorporated into PCL in the form of nanoparticles [22–24]. The current fabrication techniques of drug-laden PCL nanoparticles, namely, emulsion solvent extraction/evaporation, phase separation, and spray drying, unfortunately could only achieve low drug loading efficiency and produce scaffolds with one sole function of controlled drug release [25]. Failure to remove the organic solvents, such as methylene chloride, methanol, acetone, and ethyl acetate, used in these methods postfabrication also present significant toxicological concerns [26].

In addition to targeted drug delivery, PCL has also been extensively used in the field of tissue engineering to provide specific microarchitecture and in vivo mechanical support for the regeneration of damaged cells or tissues [27]. Conventional methods of three-dimensional scaffold fabrication,

such as gas formation, phase separation, porogen leaching, and emulsion-free drying, that fail to offer flexibility and control over the design of scaffold architecture and pore interconnectivity have been slowly replaced by the rapid prototyping system in recent years [28, 29]. Capable of providing easier and greater manipulation over the scaffold porosity and dimension, the equipment of the rapid prototyping system is, however, exorbitant and sophisticated, making its adaptation into the laboratory costly and difficult.

While PCL has demonstrated tremendous potentials in both targeted drug delivery and tissue engineering, there are limited studies that combine these two distinct functions of PCL. The drug-laden PCL nanoparticles used in targeted drug delivery often possess no other function than to release drugs, while the three-dimensional PCL scaffolds developed for tissue engineering usually contain no drug. The term tissue engineering therapeutics has been coined to describe the emerging field of three-dimensional scaffolds with additional drug delivery properties [30]. Numerous therapeutic agents, including growth factors, antibiotics, and anti-inflammatories, have been successfully loaded into three-dimensional bioactive scaffolds and demonstrated clinical potentials in the treatment and management of bone-related pathologies [31].

In this study, a biodegradable porous drug-laden PCL scaffold, which can serve as both targeted drug delivery device and mechanical support for cellular regeneration, was developed. A novel solvent-free fabrication procedure involving press-molding with poly(ethylene glycol) diacrylate (PEGDA) microneedle arrays was successfully devised. Rhodamine B was chosen as a model drug for the drug release kinetic study and to investigate the effects of surface architecture, created using microneedle arrays of varying diameters and center-to-center spacings, and drug loading concentration on the rate of drug release. To demonstrate the drug-delivering potentials of the scaffold, doxorubicin and lidocaine hydrochloride were incorporated into the scaffolds and their release profiles were determined. Lastly, a cell attachment study with human dermal fibroblasts (HDF) was carried out to examine the scaffold's ability in supporting cellular attachment.

Materials and methods

Materials

PCL (Mn=10,000), PEGDA (MW=258), 2-hydroxy-2-methylpropiophenone (97 %), 3-[tris(trimethylsilyloxy)-silyl]propyl methacrylate, lidocaine hydrochloride, and In Vitro Toxicology Assay Kit, XTT-based were purchased from Sigma-Aldrich (St. Louis, MO, USA). Rhodamine B was purchased from Alfa Aesar (Lancaster, UK).

274

Drug Deliv. and Transl. Res. (2012) 2:272–283

Doxorubicin was purchased from MP Bio (California, USA). Phosphate-buffered saline (PBS; 10×, pH 7.4) was procured from Vivantis Technologies (Kuala Lumpur, Malaysia). HDF cells were obtained from the Institute of Medical Biology, Singapore.

Fabrication of PEGDA microneedle array

The detailed fabrication procedures of the PEGDA microneedle array via soft photolithography have been reported [32]. The microneedle fabrication steps employed in this paper were similar to the reported procedures, with slight modifications. Briefly, microscopic glass slide (Sail Brand, China), previously coated with 3-[tris(trimethylsilyloxy)-silyl]propyl methacrylate overnight, was placed on a stage formed by placing two coverslips (Cell Path, Wales, UK) on a piece of glass slide. Pre-polymer solution (PEGDA and 0.5 % w/w of 2-hydroxy-2-methylpropiophenone) was inserted into the gap between the coverslips and the coated glass slide with a micropipette. The setup was irradiated with high-intensity ultraviolet (UV) light of 12.4 W/cm^2 for 1 s at a distance of 11.5 cm below the light source using EXFO OmniCure® S200-XL UV curing station (EXFO, Photonic Solutions Inc., Canada). The glass slide with the polymerized PEGDA backing was then removed from the setup and placed on another stage formed by placing two microscopic slides on a piece of glass slide. Pre-polymer solution was then inserted into the gap. An inked plastic film (photomask) containing transparent circle array (Infinite Graphics Pte. Ltd., Singapore) was placed on top of the PEGDA-coated slide and was subsequently irradiated under UV light of 12.4 W/cm^2 for 1.3 s at a distance of 2.5 cm below the light source to form the microneedles. The photomask was removed and the setup was rinsed under water to remove excess pre-polymer solution. Finally, the microneedle array was detached from the setup.

Fabrication of porous PCL scaffold

The porous scaffolds were fabricated via a press-molding technique with PEGDA microneedle arrays. First, 10 mg of PCL pellets was put onto a piece of glass slide and placed on an electric heater at 90 °C. Tweezers were utilized to spread the molten pellets. Once the molten pellets were spread, the glass slide was removed from the electric heater and an additional glass slide was used to further compress the molten polymer. The additional glass slide was removed when PCL solidified and the pressed sheet was heated up again. Once the PCL melted, the glass slide was removed from the electric heater and a PEGDA microneedle array was used to press on top of the molten PCL. The microneedle array was removed from the glass slide when the scaffold solidified. Scaffolds of different pore dimensions were created using microneedle

arrays of varying needle diameter and center-to-center spacing. A schematic of the fabrication process is shown in Fig. 1.

Morphology observation

The scaffolds were observed via phase contrast microscopy using a Nikon Eclipse Ti Inverted Research Microscope (Nikon, Japan) to determine the number and diameter of the pores created and to examine the degree of successful penetration. Photographic images of the fabricated scaffolds were obtained at SBIC Nikon Imaging Center, Biopolis, Singapore using a Nikon SMZ 1500 stereomicroscope.

Drug loading

Rhodamine B was chosen to be used in the in vitro drug release studies because it possesses a distinctive and strong absorption peak, which allows for accurate concentration analysis via UV–visible light spectroscopy [33]. The
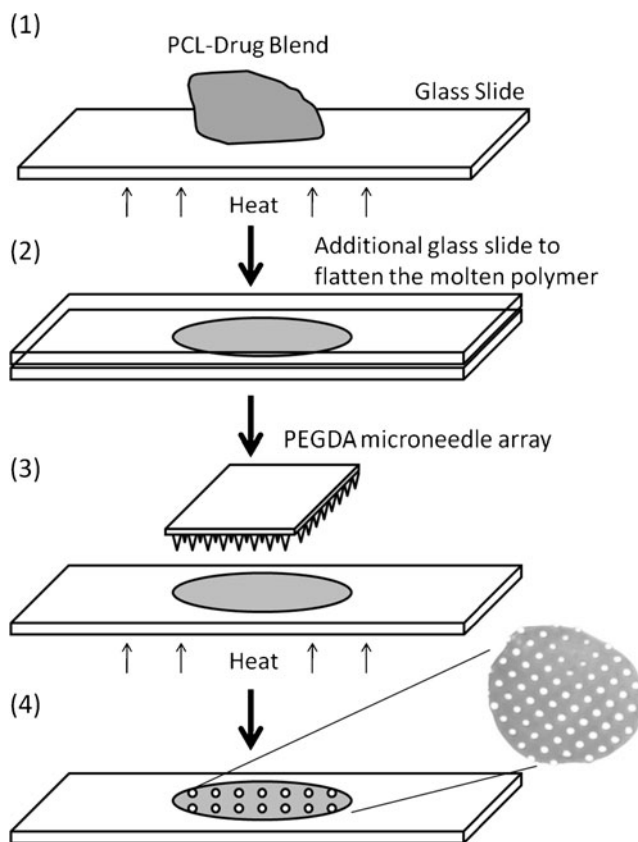
Fig. 1 Schematic of scaffold fabrication process. *1* 10 mg of PCL pellet is placed onto a piece of glass slide on an electric heater at 90 °C. The pellet is spread with tweezers. *2* The glass slide is removed from the heater. The molten polymer is compressed with another piece of glass slide. *3* The additional glass slide is removed when PCL solidifies and the pressed sheet is heated up again. Once the PCL melts, the glass slide is removed from the heater and a PEGDA microneedle array is pressed on top of the molten PCL. *4* The microneedle array is removed from the glass slide when the scaffold solidifies

fluorescence and colored property of rhodamine B also enables the observation of drug distribution in the scaffold post-fabrication with fluorescence microscopy. A measured amount of rhodamine B was added to a measured amount of PCL in a beaker placed on top of an electrical heater at 90 °C. A metal spatula was used to mix the content to obtain a homogenous blend, which was then flattened and cooled to obtain a thin sheet of stock material for scaffold fabrication. Similar procedures were employed for the encapsulation of doxorubicin and lidocaine hydrochloride.

In vitro drug release study

The effects of surface architecture and drug loading concentration on the rate of rhodamine B release were investigated. Rhodamine B–PCL scaffold was placed in a 1.5-ml microfuge tube filled with 1.0 ml of 1× phosphate buffer solution at pH 7.4. Aluminum foil was used to wrap the tube to minimize photochemical degradation, and the tube's opening was sealed with Parafilm to prevent solvent evaporation during incubation. The entire setup was placed in a rack and put in an incubator at 37.0 °C. At regular time interval, 0.5 ml aliquot of the sample was withdrawn for concentration analysis; 0.5 ml of fresh PBS was added to replenish and to maintain the total dissolution volume at 1 ml after each withdrawal. The amount of rhodamine B released was measured spectroscopically with a 96-well plate reader at 554 nm (Tecan Infinite M200, Singapore). Triplicates were performed. Similar procedures were adopted to determine the drug release profiles of doxorubicin and lidocaine hydrochloride. Spectroscopic analysis of doxorubicin was performed using the Tecan plate reader at 485 nm, while lidocaine hydrochloride was analyzed with a UV spectrophotometer (Shimadzu UV1800) at 216.5 nm.

Mathematical model fitting

The release data of rhodamine B were fitted in the zero-order, first-order, Hixson–Crowell, and Higuchi mathematical models. The goodness of fit was determined by comparing the average R^2 values generated from simple linear regression. The model that best fit the data was chosen to calculate the arbitrary release constants for the various drug release profiles, which were then used to compare the rates of drug release from scaffolds of varying pore dimensions and drug loading concentrations. In addition, the data were also fitted to the Korsmeyer–Peppas model to determine the average release exponent.

Cell attachment study

HDF were cultured in Dulbecco's modified Eagle's medium (Invitrogen, California, USA) supplemented with 1 % penicillin/streptomycin (PAN-Biotech, Aidenbach, Bavaria, Germany) and 10 % fetal bovine serum (Invitrogen, California, USA) at 37 °C and 5 % CO_2. Blank porous scaffolds, fabricated with microneedle arrays of 400 μm needle diameter and 2× diameter center-to-center spacing, were immersed in 70 % ethanol overnight, followed by thorough rinsing with sterile PBS. The scaffolds were then placed into the wells of a nontissue culture-treated 96-well plate (Nunc, Roskilde, Denmark). Cell suspensions consisting of 10^4 cells were seeded onto the scaffolds and additional culture medium were added to top up the well volume to 200 μL. Culture media were changed every 3 days and the cultures were maintained for 5 days.

On days 2 and 5, the cultures were examined for cell attachment via an XTT assay. Briefly, culture media were first removed from the wells via a micropipette and the wells were washed thoroughly with sterile PBS. Two hundred microliters of PBS was then added into the wells together with 40 μL of XTT solution (0.5 mg/ml). One hundred microliters of the samples were withdrawn and placed into a new 96-well plate after 5 h of incubation and their absorbance at 450 nm were determined with a plate reader.

A negative control, which involves cell seeding in a 96-well plate without tissue culture treatment or PCL scaffold, and a positive control, which involves cell seeding in a 96-well plate with tissue culture treatment (Corning Incorporated, Corning, NY, USA) but no PCL scaffold, were conducted.

Statistical analysis

One-way analysis of variance was conducted using SPSS, while linear regression and graph plotting were performed in Microsoft Excel Software.

Results

Scaffold fabrication

Porous PCL scaffolds were successfully fabricated using the method illustrated in Fig. 1. The porous scaffolds formed from 10 mg of PCL were white in color and resembled a flattened circular sheet, with a diameter and height of approximately 8 and 0.2 mm, respectively. It was observed that the average pore diameter created by the 400-μm microneedle arrays (2× diameter center-to-center spacing, 268.09 ±32.16 μm; 3× diameter center-to-center spacing, 278.51± 23.02 μm; 4× diameter center-to-center spacing, 287.72± 29.64 μm; 5× diameter center-to-center spacing, 286.67± 26.16 μm) were the highest, followed by the 300-μm microneedle arrays (2× diameter center-to-center spacing, 187.17 ±38.13 μm; 3× diameter center-to-center spacing, 172.15±

276

Drug Deliv. and Transl. Res. (2012) 2:272–283

29.56 μm; 4× diameter center-to-center spacing, 192.97±29.87 μm; 5× diameter center-to-center spacing, 169.33±31.19 μm) and the 200-μm microneedle arrays (2× diameter center-to-center spacing, 93.91±27.26 μm; 3× diameter center-to-center spacing, 84.31±24.23 μm; 4× diameter center-to-center spacing, 97.38±25.74 μm; 5× diameter center-to-center spacing, 85.91±16.54 μm). The center-to-center spacing of the microneedle arrays showed no significant effect on the average diameter of the pores created ($p > 0.05$ for all three different microneedle base diameters).

The microscopic images of the fabricated scaffolds are shown in Fig. 2. The number of pores created decreased with increasing microneedle base diameter and center-to-center spacing. It was also observed that the pores created by the 200-μm microneedle arrays were more distorted and not fully penetrated.

Rhodamine B release profiles

The effect of scaffold pore dimension on the rate of rhodamine B release is illustrated in Fig. 3a. The concentration of rhodamine B within the scaffolds was fixed to be 0.5 % w/w. The percentage cumulative release of rhodamine B increased steadily over a period of 112 days. A subsequent concentration analysis done at the end of 10 months demonstrated negligible rhodamine B release (data not shown). Generally, the effects of different microneedle center-to-center spacings on the rate of drug release were inconspicuous and all scaffolds loaded with the same amount of rhodamine B achieved comparable plateau level of percentage cumulative release at the end of 10 months (data not shown). Nonetheless, on closer inspection, it was observed that the scaffolds fabricated with the 300- and 400-μm microneedle arrays demonstrated increasing drug release rate with decreasing microneedle center-to-center spacing at the initial stage of drug release before the common plateaus were reached. The differences were more conspicuous in scaffolds fabricated with the 400-μm microneedle arrays.

Figure 3b depicts the rhodamine B release profiles of scaffolds with varying drug concentrations over 112 days The release of rhodamine B, both cumulative and

Fig. 2 Microscopic images of the scaffolds fabricated using microneedle arrays of varying needle base diameters and center-to-center spacings. Increasing microneedles base diameter from 200 to 400 μm increases the pore size and reduces the number of pores formed. Increasing microneedles center-to-center spacing from 2× to 5× diameter reduces the number of pores formed
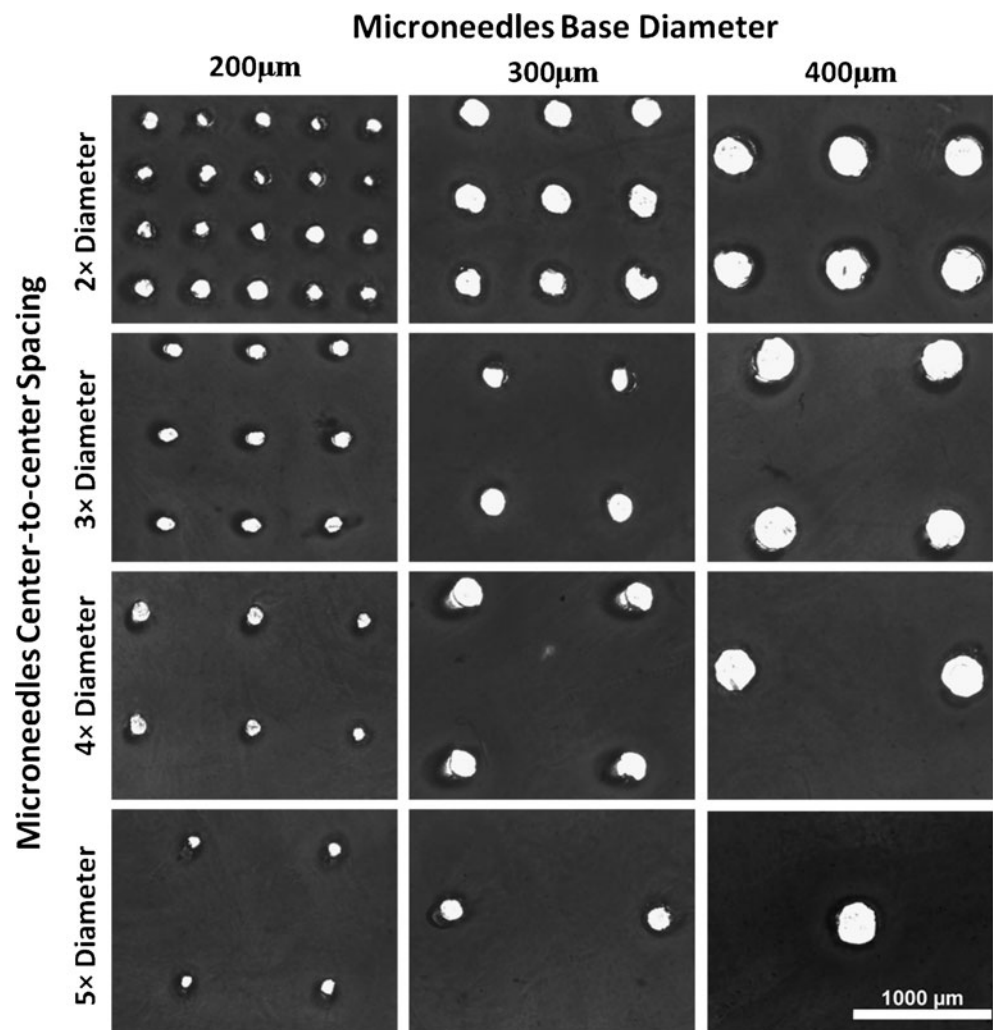
Fig. 3 In vitro drug release studies. **a** Percentage cumulative rhodamine B release over 112 days for different scaffold pore dimensions formed from microneedle arrays with microneedle-based diameters ranging from 200 to 400 μm and center-to-center spacing ranging from 2× to 5× diameter. Drug concentration in scaffolds was fixed at 0.5 %. **b** Cumulative rhodamine B release and percentage cumulative rhodamine B release over 112 days for different drug loading concentrations from scaffolds formed from microneedle arrays with microneedle-based diameter of 400 μm and center-to-center spacing of 2× diameter

percentage cumulative, increased gradually over time. Again, a subsequent concentration analysis of the samples at the end of 10 months showed negligible drug release and plateaus were obtained (data not shown). It was observed that the rate of cumulative release increased with increasing drug loading concentration, while the rate of percentage cumulative release increased with decreasing drug loading concentration.

Mathematical model fitting

The release profiles of rhodamine B fit the Higuchi model best, as indicated by the highest R^2 obtained and tabulated in Fig. 4a. The release constant, k, for the various sets of experiment was generated using the Higuchi model. Figure 4b shows a plot of k across different drug loading concentrations. It was observed that k decreased with increasing drug loading concentration. The bar chart of k against different microneedle center-to-center spacings revealed that, with the exception of scaffolds fabricated using the 200-μm microneedle arrays, k decreased with increasing microneedle center-to-center spacings and the decrease was more stark in the scaffolds fabricated using the 400-μm microneedle arrays. These findings were consistent with the observations made earlier with the drug release profiles.

Doxorubicin and lidocaine hydrochloride release

The release profiles of doxorubicin and lidocaine hydrochloride from PCL, together with that of rhodamine B, are shown in Fig. 5a. The drug loading concentration used for all scaffolds was 0.5 % w/w and all scaffolds were fabricated using microneedle arrays with 400 μm needle diameter and 2× diameter center-to-center spacing. Two distinct release patterns were observed, in which rhodamine B and doxorubicin were released in a slow and sustained manner, while lidocaine hydrochloride demonstrated rapid release. The release of doxorubicin was significant lower than that of rhodamine B, achieving only 7 % release on day 56, as shown in Fig. 5b. The cumulative release of doxorubicin from

278

Drug Deliv. and Transl. Res. (2012) 2:272–283

a

Mathematical Model	Equation	Mean R^2
Zero Order	$y = kt$	0.1852
First Order	$\ln(100-y) = -kt$	0.6016
Hixson Crowell	$100-(100-y)^{1/3} = kt$	0.4714
Higuchi	$y = kt^{0.5}$	0.8598

y denotes cumulative percentage release and k denotes constant of the respective mathematical model.

b
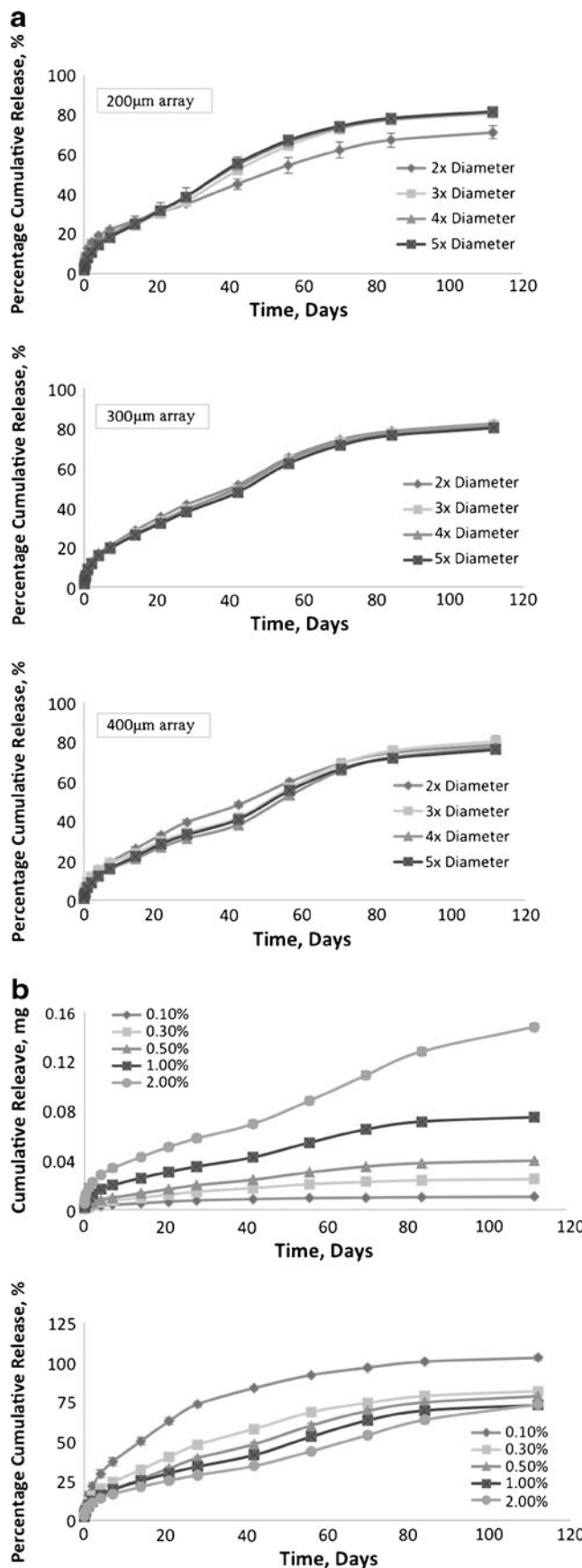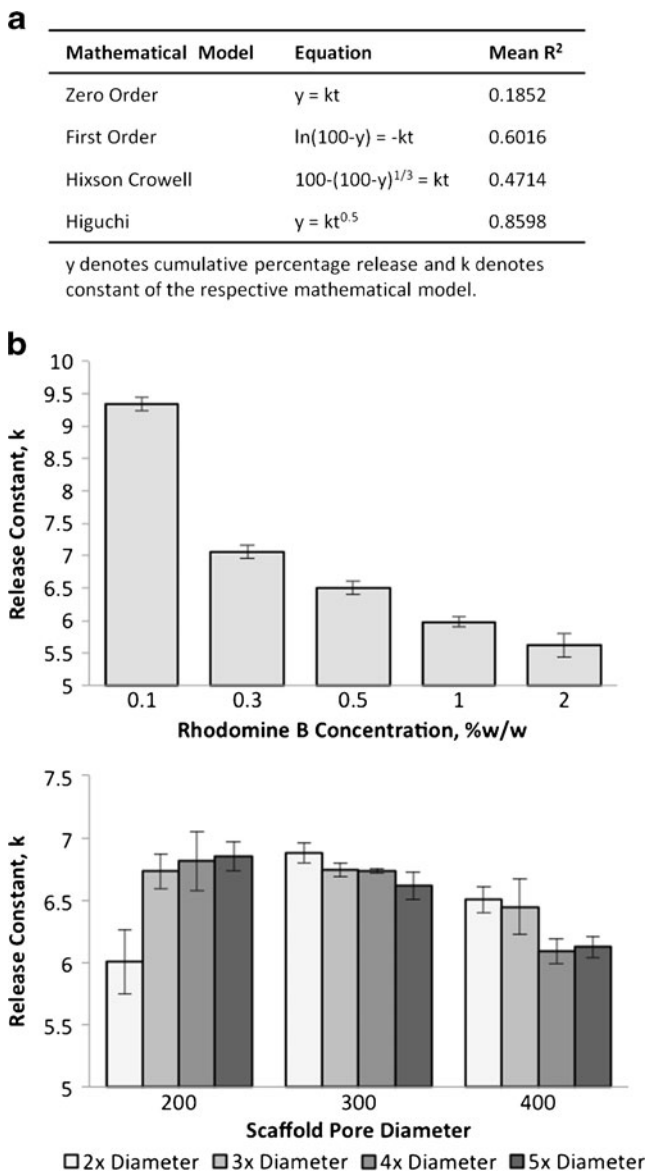
Fig. 4 **a** Mathematical model equations and fitting results. Release kinetics were found to fit the Higuchi model best. **b** Graphs of diffusion constant, k, across different drug loading concentrations and different scaffold pore dimensions. Increasing rhodamine B scaffold concentration decreases the k value. Increasing microneedle-based diameter and center-to-center spacing decrease the k value

the scaffolds was further investigated and it was revealed in Fig. 5c that doxorubicin demonstrated initial rapid release followed by slow and sustained release afterwards.

Cell attachment study

While it was revealed that the PCL scaffolds were able to provide attachment surfaces for the HDF, as evidenced by the higher cell viability obtained as compared to the negative control in Fig. 6, the scaffolds were unable to achieve the same degree of cellular attachment provided by the positive control.
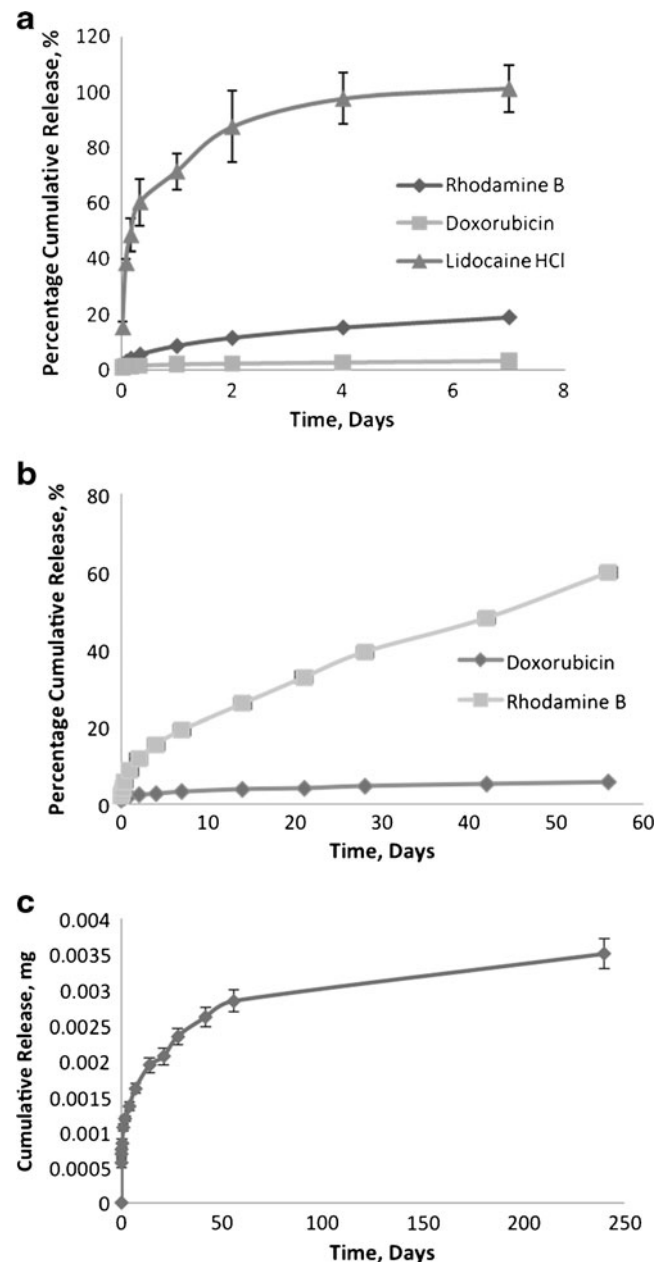
Fig. 5 **a** Percentage cumulative release of rhodamine B, doxorubicin, and lidocaine hydrochloride over 7 days. Lidocaine hydrochloride showed rapid and complete release within a week, while rhodamine B and doxorubicin demonstrated sustained release. **b** Percentage cumulative release of rhodamine B and doxorubicin over 56 days. The percentage of drug release was higher for rhodamine B- than doxorubicin-loaded scaffolds by day 56. **c** Cumulative release of doxorubicin over 240 days. Initial burst release followed by slow and sustained release were observed

Discussion

Scaffolds fabrication

The scaffolds' pore sizes are affected by the diameter of the microneedle arrays. The larger the microneedle base

Drug Deliv. and Transl. Res. (2012) 2:272–283

279
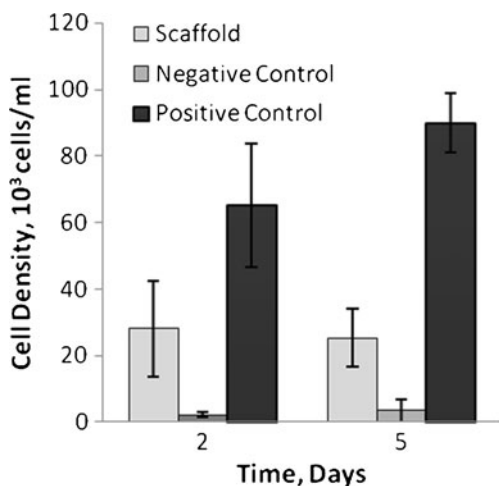
Fig. 6 In vitro cell attachment study on PCL scaffolds with HDF. Cell attachments were observed on the scaffolds but not in the negative control (nontissue culture-treated 96-well plate without scaffold). Cell attachments on positive control (tissue culture-treated 96-well plate without scaffold) were higher than that on the scaffolds

diameter, the larger the pore diameter. Microneedle center-to-center spacing and base diameter determine the number of pores formed on the scaffold. As microneedle arrays with larger center-to-center spacing and higher diameter possess fewer individual needles per unit area, the resultant scaffolds formed from these arrays would contain fewer pores as compared to those fabricated using arrays with smaller microneedle center-to-center spacing and microneedle diameter. As the base diameter and the center-to-center spacing of the microneedle arrays can be easily adjusted by changing the photomasks used to fabricate the microneedles, this press-molding technique developed can, therefore, be used to produce scaffolds with different surface architectures with great ease and flexibility.

Fabricating scaffolds using microneedle arrays with 200 μm needle base diameter were particularly challenging. Arrays with larger center-to-center spacing were generally more fragile, as the individual needles are thinner and are separated at greater distance from each other. Arrays with smaller center-to-center spacing, on the other hand, lacked uniformity and often fused at certain spots, possibly due to insufficient spacing between adjacent needles and limited UV penetration across smaller transparent circles on the photomasks. All these factors contributed to the variable pore size and poor degree of penetration on scaffolds fabricated with 200 μm microneedle arrays.

Microneedle arrays with 400 μm diameter and 2× diameter center-to-center spacing were observed to possess the highest mechanical strength and were found to be the easiest to fabricate and work with. In addition, they also produce scaffolds with consistent pore diameter and penetration. As such, for the subsequent experiments, except the study on the effects of different scaffold pore dimensions on the rate

of drug release, microneedle arrays with 400 μm needle diameter and 2× diameter center-to-center spacing were chosen to fabricate the scaffolds.

Unlike the other existing drug-laden nanoparticles fabrication techniques, no organic solvent was used in the fabrication process developed in this study, thereby eliminating the need to remove solvent post-fabrication. However, as a temperature of at least 60 °C is required to melt PCL, this fabrication technique might not be suitable for the encapsulation of chemical drugs and proteins that are susceptible to thermal degradation.

Mathematical model fitting and drug release mechanism

Different drug release models represent different drug release mechanisms. The zero-order kinetic states that the rate of drug release is directly proportional to time and can be used to describe the release of drugs with low solubility from a matrix tablet system [34]. The first-order kinetic suggests that the rate of drug release is directly proportional to the amount of drug remaining in the system and is useful in explaining the release of drugs dispersed in a porous matrix system [35]. The Hixson–Crowell model describes the release of drugs by dissolution associated with a change in the surface and volume of particles or tablet [36]. The Higuchi model, which was derived from the Fick's first law of diffusion, states that the release of drug is governed by simple diffusion [37].

From the experiments and mathematical model fitting conducted, it can be deduced that the release of rhodamine B from PCL follows simple diffusion as described by the Higuchi model, in which solvent would first penetrate the scaffold, dissolve the drug loaded within, and release the dissolved drug into the acceptor solution. The result from the Korsmeyer–Peppas model, which gave an average exponent value of 0.427 (<0.45), further indicates that the release of rhodamine B from PCL follows simple Fickian diffusion [38].

The diffusion constant, k, of the various sets of experiments was calculated using the Higuchi model. Higher k value indicates faster drug release and vice versa. The use of k values allows for clearer visual comparison between the different release profiles. This was useful especially since the release profiles obtained for scaffolds fabricated with varying microneedles dimension were rather close to each other, with differences occurring primarily at the initial phase of drug release before the plateau was attained.

Effects of scaffold surface architecture on rhodamine B release

Comparison between the different k values calculated suggested that, with the exception of scaffolds fabricated with the 200-μm microneedle arrays, the rate of drug release, as

280

Drug Deliv. and Transl. Res. (2012) 2:272–283

indicated by k, decreased as the center-to-center spacing of the microneedle arrays used increased. In general, microneedle arrays with higher center-to-center spacing produce scaffolds with fewer pores and hence smaller total surface area. Since the rate of diffusion is directly proportional to the surface area, scaffolds with a lower surface area, fabricated using microneedle arrays of higher center-to-center spacing, would demonstrate a slower rate of drug release.

Aside from center-to-center spacing, the microneedle diameter also contributed to the overall rate of drug release. It was observed that the larger the diameter of the microneedles used in fabrication, the slower the rate of drug release. While microneedle arrays of a larger diameter are able to produce scaffolds with larger pores, the fewer number of pores created, as compared to those fabricated with microneedle arrays of smaller diameter, still lead to a lower scaffold surface area and thus slower rate of drug release.

A multiple linear regression analysis conducted to correlate the three factors, namely, k, microneedles base diameter, and microneedles center-to-center spacing, for the release data of scaffolds fabricated with the 300- and 400-μm microneedle arrays revealed a significant negative linear relationship between the variables ($R^2=0.725$). Increasing microneedles diameter and center-to-center spacing lead to decreasing k and hence rate of drug release. The less than desired R^2 value obtained, however, could be indicative that the relationship between the variables is not purely linear.

The drug release data of the scaffolds fabricated using the 200-μm microneedle arrays were not consistent with the expected trend and were observed to be more erratic and variable. This discrepancy could be due to the technical inconsistencies of fabricating microneedle arrays with smaller needles diameter, which presented great difficulties in controlling the scaffold surface area. Moreover, the close proximity and limited spacing between the individual needles on the 200-μm microneedle arrays, especially for arrays with 2× diameter center-to-center spacing, often produced arrays with fused patches that tend to adsorb rhodamine B preloaded into the polymer, as evidenced by the pink stains observed on the microneedle arrays post scaffold fabrication, leading to significant drug loss and hence slower apparent rate of drug release.

Effects of drug loading concentration on rhodamine B release

The scaffold surface architecture was fixed in this experiment in order to examine the effect of varying drug loading concentrations on the rate of drug release. As the scaffold pore dimension was observed previously to have limited consequences on the rate of drug release, microneedle arrays of 400 μm needle diameter and 2× center-to-center spacing were chosen to be used in this experiment to fabricate the scaffold as they have shown to be capable of producing scaffolds with consistent pore dimensions and are relatively easier to work with as compared to those arrays with smaller microneedle diameter and larger center-to-center spacing.

Increasing drug loading concentration has a positive relationship on the cumulative release of rhodamine B. This is because, as drug loading concentration increases, the amount of drug present in the scaffold also increases, resulting in a steeper diffusion gradient between the scaffolds and the surrounding dissolution media, leading to increased rate of diffusion and drug release.

An opposite trend, however, was obtained for the plot of percentage cumulative release. This is postulated to be due to rhodamine B being preferentially adsorbed on the surface, instead of being embedded in the core of the polymer. Drugs on scaffold surface would first be dissolved and be released into the dissolution medium during drug release. Since a higher proportion of drug in scaffolds with lower drug loading concentration is present on the surface, whatever released from the scaffold, even if the absolute amount may be low, would account for a huge percentage of drug loss from the total amount of drug incorporated.

Release profiles of doxorubicin and lidocaine hydrochloride

The scaffolds developed demonstrated promising potential in encapsulating different types of drugs for targeted drug delivery. The release of doxorubicin was observed to be significantly slower than that of rhodamine B, possibly due to the limited solubility of doxorubicin in PBS at pH 7.4 that retarded the rate at which the drug is dissolved by the dissolution medium [39]. Unlike rhodamine B and doxorubicin, lidocaine hydrochloride demonstrated rapid and high initial burst release and was almost completely released from the scaffolds after 2 days. The difference could be attributed to the highly soluble nature of lidocaine hydrochloride salt, which greatly enhanced the rate of dissolution and hence drug release. Rhodamine B, being a relatively more hydrophilic entity, may not model the release of salts or highly polar chemicals as well as their more hydrophobic counterparts. In order to better predict the release characteristics of salts, other model compounds may be needed.

Cell attachment study

HDF were chosen for the cell attachment study as HDF have demonstrated the ability to differentiate along an osteoblastic linage [40] and can be isolated with greater ease and less invasiveness as compared to conventional osteoblasts used in bone tissue engineering [41].

Two different types of tissue culture plates were employed in this study, namely, the tissue culture-treated plate and the

nontissue culture-treated plate. The term "tissue culture-treated" refers to treatment procedures, like corona discharge or gas–plasma, that render the material surface more hydrophilic, via the generation of energetic oxygen ions that attach to the material surface, and therefore, more favorable for cellular attachment [42]. Nontissue culture plates, on the other hand, offer hydrophobic surfaces and are often chosen for the culturing of cells where cellular attachments are to be minimized or avoided.

In this experiment, a negative control, which involved the seeding of HDF in a nontissue culture-treated plate, was conducted to demonstrate that the cellular growth observed in the experiment set, which involved the seeding of HDF in a nontissue culture plate with PCL scaffolds, is due to the attachment surfaces provided by the scaffold per se. In the presence of PCL scaffolds, HDF growth and attachment were observed to be significantly higher than that of the negative control, suggesting that the scaffolds are capable of providing the cells with suitable sites for attachment. The attachment, however, was better in the positive control because anchorage-dependent cells, such as HDF, do not grow and attach on hydrophobic surfaces well [43] and PCL, being a highly hydrophobic polymer, is unable to provide a cell-attaching environment that is as ideal as those provided by the tissue culture-treated plates.

Potential clinical applications

The scaffold developed in this paper could potentially perform similar function to those orthopedic devices and act as a cell attachment site for the regeneration and growth of healthy bone cells. Long-term in vivo studies have demonstrated that the PCL implant was able to maintain its physical shape after 2 years of implantation. In addition, PCL was also shown to be capable of being degraded into low molecular pieces at the end of 30 months and be excreted out of the body completely, without accumulating in the body tissues [44]. The slow degradation rate and biodegradable property of PCL makes it ideal to be developed into implants that could support long-term tissue regeneration.

As a targeted drug delivery system, the scaffolds can be used to encapsulate anticancer drugs such as doxorubicin and cisplatin to prevent cancer recurrence and minimize systemic toxicity. Other agents, including antibiotics, anticoagulants, opioids, mild narcotics, anti-inflammatory, and analgesics, can also be incorporated into the scaffolds and be released to the surrounding tissues, reducing the need for daily dosing and possible systemic side effects.

One concern regarding the use of this dual-function scaffold lies on the influence of the cytotoxic agent like doxorubicin on bone cells attachment and regeneration. In a clinical setting, intensive chemotherapy following limb salvage surgery is warranted to eradicate remaining malignant deposits. Unfortunately, bone healing occurs simultaneously with the administration of systemic chemotherapy. While postsurgical chemotherapy has been shown to improve relapse-free survival time of patients with certain primary osteosarcomas, postoperative chemotherapy does indeed affect bone growth and bone healing [45, 46]. As for the treatment regimen, most patients would be placed on doxorubicin 25 mg/m^2/day on days 1 to 3 and cisplatin 100 mg/m^2 on day 1, every 3 weeks for six cycles [47–49]. Other options include the control arm of the AOST0331 protocol (methotrexate, doxorubicin and cisplatin (MAP) chemotherapy) which involves 10 weeks of preoperative and 18 weeks of postoperative chemotherapy with doxorubicin, cisplatin, high-dose methotrexate, and leucovorin rescue (protocol information available online at www.cancer.gov/clinicaltrials/COG-AOST0331). Generally, 18 weeks (around 126 days) of intermittent postoperative chemotherapy are required. While the scaffolds developed in this paper could potentially face the same problem of growth inhibition induced by the release of chemotherapeutic agents like doxorubicin, they have successfully demonstrated initial rapid release of up to around 100 days for rhodamine B and around 60 days for doxorubicin. Specifically for rhodamine B, close to 79 % of the total drug loaded was released at the end of 112 days and only a mere additional 2 %, making to an eventual total of 81 %, was released between day 112 and day 300. Similarly for doxorubicin, approximately 6 % of the total drug content was released at the end of 56 days and only an additional 1 % was released between day 56 and day 240. With higher rate of initial release, sufficient quantity of the cytotoxic agent could be released at the implanted site to destroy lingering malignancies during the initial phase of treatment, leaving negligible amount of drug to be released afterward so that the scaffold can function primarily as a tissue engineering platform to support cell growth and bone regeneration. A study has shown that 58–580 ng/ml of doxorubicin has shown significant dose-dependent growth inhibition in a panel of human cell lines, representative for primary metastatic bone tumors [50]. The amount of drug loaded in the scaffold may be adjusted to achieve this desired local concentration after release for the initial killing of cancerous cells. Multiple chemotherapeutic agents may also be incorporated into the scaffold to better mimic conventional multidrug chemotherapy regimens.

Conclusion

A novel porous and drug-laden biodegradable PCL scaffold with high loading efficiency was developed using a simple, inexpensive, and solvent-free press-molding technique with PEGDA microneedle arrays. It has been shown that the scaffolds were able to release rhodamine B slowly over a

period of 112 days with a simple diffusion mechanism and that the rate of drug release can be controlled by altering the drug loading concentration and the scaffold surface architecture. Two other drugs, namely, doxorubicin and lidocaine hydrochloride, were also successfully incorporated into the scaffolds, demonstrating the vast potential of the scaffolds to be an effective targeted drug delivery system. The positive result of the cell attachment study also verified the ability for the scaffold to support cellular attachment.

References

1. Lindell EB, Carroll NC. Limb salvage tumor surgery in children. Iowa Orthop J. 1993;13:124–35.
2. Messerschmitt PJ, Garcia RM, Abdul-Karim FW, Greenfield EM, Getty PJ. Osteosarcoma. J Am Acad Orthop Surg. 2009;17 (8):515–27.
3. Carty CP, Dickinson IC, Watts MC, Crawford RW, Steadman P. Impairment and disability following limb salvage procedures for bone sarcoma. Knee. 2009;16(5):405–8..
4. Agins HJ, Alcock NW, Bansal M, Salvati EA, Wilson Jr PD, Pellicci PM, et al. Metallic wear in failed titanium-alloy total hip replacements. A histological and quantitative analysis. J Bone Joint Surg Am. 1988;70(3):347–56.
5. Lalor PA, Revell PA, Gray AB, Wright S, Railton GT, Freeman MA. Sensitivity to titanium. A cause of implant failure? J Bone Joint Surg Br. 1991;73(1):25–8.
6. Uhthoff HK, Finnegan M. The effects of metal plates on post-traumatic remodelling and bone mass. J Bone Joint Surg Br. 1983;65(1):66–71.
7. Yaremchuk MJ, Fiala TG, Barker F, Ragland R. The effects of rigid fixation on craniofacial growth of rhesus monkeys. Plast Reconstr Surg. 1994;93(1):1–10. discussion 1–5.
8. Sullivan PK, Smith JF, Rozzelle AA. Cranio-orbital reconstruction: safety and image quality of metallic implants on CT and MRI scanning. Plast Reconstr Surg. 1994;94(5):589–96.
9. Dhillon MS, Prabhakar S, Prasanna C. Preliminary experience with biodegradable implants for fracture fixation. Indian J Orthop. 2008;42(3):319–22.
10. Mankin HJ, Gebhardt MC, Jennings LC, Springfield DS, Tomford WW. Long-term results of allograft replacement in the management of bone tumors. Clin Orthop Relat Res. 1996;324:86–97.
11. Moore WR, Graves SE, Bain GI. Synthetic bone graft substitutes. ANZ J Surg. 2001;71(6):354–61.
12. Kurz LT, Garfin SR, Booth Jr RE. Harvesting autogenous iliac bone grafts. A review of complications and techniques. Spine (Phila Pa 1976). 1989;14(12):1324–31.
13. Schantz JT, Lim TC, Ning C, Teoh SH, Tan KC, Wang SC, et al. Cranioplasty after trephination using a novel biodegradable burr hole cover: technical case report. Neurosurgery. 2006;58(1 Suppl): ONS-E176. discussion ONS-E176.
14. Schuckert KH, Jopp S, Teoh SH. Mandibular defect reconstruction using three-dimensional polycaprolactone scaffold in combination with platelet-rich plasma and recombinant human bone morphogenetic protein-2: de novo synthesis of bone in a single case. Tissue Eng Part A. 2009;15(3):493–9.
15. Rosen G, Caparros B, Huvos AG, Kosloff C, Nirenberg A, Cacavio A, et al. Preoperative chemotherapy for osteogenic-sarcoma: selection of postoperative adjuvant chemotherapy based on the response of the primary tumor to preoperative chemotherapy. Cancer. 1982;49 (6):1221–30.
16. Susa M, Iyer AK, Ryu K, Hornicek FJ, Mankin H, Amiji MM, et al. Doxorubicin loaded polymeric nanoparticulate delivery system to overcome drug resistance in osteosarcoma. BMC Cancer. 2009;9:399.
17. Hogendoorn PC, Athanasou N, Bielack S, De Alava E, Dei Tos AP, Ferrari S, et al. Bone sarcomas: ESMO clinical practice guidelines for diagnosis, treatment and follow-up. Ann Oncol. 2010;21 Suppl 5:v204–13.
18. Matsumine A, Takegami K, Asanuma K, Matsubara T, Nakamura T, Uchida A, et al. A novel hyperthermia treatment for bone metastases using magnetic materials. Int J Clin Oncol. 2011;16 (2):101–8.
19. Gaur AH, Liu T, Knapp KM, Daw NC, Rao BN, Neel MD, et al. Infections in children and young adults with bone malignancies undergoing limb-sparing surgery. Cancer. 2005;104(3):602–10.
20. Goff BJ, Castillo R, Raja SN. Painful sequelae following limb salvage: etiology and management. J Am Acad Orthop Surg. 2011;19 Suppl 1:S23–7.
21. Kumari A, Yadav SK, Yadav SC. Biodegradable polymeric nanoparticles based drug delivery systems. Colloids Surf B Biointerfaces. 2010;75(1):1–18.
22. Gou M, Zheng X, Men K, Zhang J, Zheng L, Wang X, et al. Poly (epsilon-caprolactone)/poly(ethylene glycol)/poly(epsilon-caprolactone) nanoparticles: preparation, characterization, and application in doxorubicin delivery. J Phys Chem B. 2009;113 (39):12928–33.
23. Li X, Li R, Qian X, Ding Y, Tu Y, Guo R, et al. Superior antitumor efficiency of cisplatin-loaded nanoparticles by intratumoral delivery with decreased tumor metabolism rate. Eur J Pharm Biopharm. 2008;70(3):726–34.
24. Teo EY, Ong SY, Chong MS, Zhang Z, Lu J, Moochhala S, et al. Polycaprolactone-based fused deposition modeled mesh for delivery of antibacterial agents to infected wounds. Biomaterials. 2011;32(1):279–87.
25. Takada K. Microfabrication-derived DDS: from batch to individual production. Drug Discov Ther. 2008;2(3):140–55.
26. Lin W-J, Flanagan DR, Linhardt RJ. A novel fabrication of poly(ε-caprolactone) microspheres from blends of poly(ε-caprolactone) and poly(ethylene glycol)s. Polymer. 1999;40(7):1731–5.
27. Khademhosseini A, Vacanti JP, Langer R. Progress in tissue engineering. Sci Am. 2009;300(5):64–71.
28. Kim GH, Son JG. 3D polycarprolactone (PCL) scaffold with hierarchical structure fabricated by a piezoelectric transducer (PZT)-assisted bioplotter. Appl Phys A Mater. 2009;94 (4):781–5.
29. Park SA, Lee SH, Kim WD. Fabrication of porous polycaprolactone/ hydroxyapatite (PCL/HA) blend scaffolds using a 3D plotting system for bone tissue engineering. Bioprocess Biosyst Eng. 2011;34 (4):505–13.
30. Baroli B. From natural bone grafts to tissue engineering therapeutics: brainstorming on pharmaceutical formulative requirements and challenges. J Pharm Sci. 2009;98(4):1317–75.
31. Mouriño V, Boccaccini AR. Bone tissue engineering therapeutics: controlled drug delivery in three-dimensional scaffolds. J R Soc Interface. 2010;7(43):209–27.
32. Kochhar JS, Goh WJ, Chan SY, Kang L. A simple method of microneedle array fabrication for transdermal drug delivery. Drug Dev Ind Pharm. 2012; in press.
33. Zhang JT, Keller TF, Bhat R, Garipcan B, Jandt KD. A novel two-level microstructured poly(N-isopropylacrylamide) hydrogel for controlled release. Acta Biomater. 2010;6(10):3890–8.

Drug Deliv. and Transl. Res. (2012) 2:272–283

283

34. Tanaka N, Imai K, Okimoto K, Ueda S, Tokunaga Y, Ibuki R, et al. Development of novel sustained-release system, disintegration-controlled matrix tablet (DCMT) with solid dispersion granules of nilvadipine (II): in vivo evaluation. J Control Release. 2006;112 (1):51–6.

35. Mulye NV, Turco SJ. A simple-model based on first-order kinetics to explain release of highly water-soluble drugs from porous dicalcium phosphate dihydrate matrices. Drug Dev Ind Pharm. 1995;21(8):943–53.

36. Hixson AW, Crowell JH. Dependence of reaction velocity upon surface and agitation: I—theoretical consideration. Ind Eng Chem. 1931;23:923–31.

37. Rodrigues MR, Lanzarini CM, Ricci E. Preparation, in vitro characterization and in vivo release of naproxen loaded in poly-caprolactone nanoparticles. Pharm Dev Technol. 2011;16(1):12–21.

38. Chang HI, Perrie Y, Coombes AG. Delivery of the antibiotic gentamicin sulphate from precipitation cast matrices of polycaprolactone. J Control Release. 2006;110(2):414–21.

39. Gou M, Shi H, Guo G, Men K, Zhang J, Zheng L, et al. Improving anticancer activity and reducing systemic toxicity of doxorubicin by self-assembled polymeric micelles. Nanotechnology. 2011;22 (9):095102.

40. Hee CK, Nicoll SB. Induction of osteoblast differentiation markers in human dermal fibroblasts: potential application to bone tissue engineering. Conf Proc IEEE Eng Med Biol Soc. 2006;1:521–4.

41. Notingher I, Jell G, Lohbauer U, Salih V, Hench LL. In situ non-invasive spectral discrimination between bone cell phenotypes used in tissue engineering. J Cell Biochem. 2004;92(6):1180–92.

42. Ramsey WS, Hertl W, Nowlan ED, Binkowski NJ. Surface treatments and cell attachment. In Vitro Cell Dev B. 1984;20(10):802–8.

43. Anselme K. Osteoblast adhesion on biomaterials. Biomaterials. 2000;21(7):667–81.

44. Sun HF, Mei L, Song CX, Cui XM, Wang PY. The in vivo degradation, absorption and excretion of PCL-based implant. Biomaterials. 2006;27(9):1735–40.

45. Morcuende JA, Gomez P, Stack J, Oji G, Martin J, Fredericks DC, et al. Effect of chemotherapy on segmental bone healing enhanced by rhBMP-2. Iowa Orthop J. 2004;24:36–42.

46. Friedlaender GE, Tross RB, Doganis AC, Kirkwood JM, Baron R. Effects of chemotherapeutic agents on bone. I. Short-term methotrexate and doxorubicin (adriamycin) treatment in a rat model. J Bone Joint Surg Am. 1984;66(4):602–7.

47. Bramwell VH, Steward WP, Nooij M, Whelan J, Craft AW, Grimer RJ, et al. Neoadjuvant chemotherapy with doxorubicin and cisplatin in malignant fibrous histiocytoma of bone: a European Osteosarcoma Intergroup study. J Clin Oncol. 1999;17 (10):3260–9.

48. Souhami RL, Craft AW, Van der Eijken JW, Nooij M, Spooner D, Bramwell VH, et al. Randomised trial of two regimens of chemotherapy in operable osteosarcoma: a study of the European Osteosarcoma Intergroup. Lancet. 1997;350(9082):911–7.

49. Bramwell VH, Burgers M, Sneath R, Souhami R, van Oosterom AT, Voute PA, et al. A comparison of two short intensive adjuvant chemotherapy regimens in operable osteosarcoma of limbs in children and young adults: the first study of the European Osteosarcoma Intergroup. J Clin Oncol. 1992;10(10):1579–91.

50. Salerno M, Cenni E, Fotia C, Avnet S, Granchi D, Castelli F, et al. Bone-targeted doxorubicin-loaded nanoparticles as a tool for the treatment of skeletal metastases. Curr Cancer Drug Targets. 2010;10(7):649–59.